Carbon Trends 9 (2022) 100209

Contents lists available at ScienceDirect

Carbon Trends

journal homepage: www.elsevier.com/locate/cartre

N-type diamane: An effective emitter layer in crystalline silicon heterojunction solar cell

Naima, Pawan K. Tyagi*, Vinod Singh

Department of Applied Physics, Delhi Technological University, New Delhi 110042, India

ARTICLE INFO

Article history:
Received 20 June 2022
Revised 9 August 2022
Accepted 27 August 2022

Keywords:
2D material
Diamane
Silicon heterojunction solar cell
AFORS-HET v 2.5 software

ABSTRACT

In the presented work, cell's parameter of heterostructure silicon solar cell modelled as: ITO (front contact)/n-Dn/p-cSi/Ag under the illumination of monochromatic light at standard spectrum AM-1.5 G, has been optimized by using AFORS-HET v 2.5 software. We have used n-type diamane as an emitter layer and the nature of diamane has been considered 3D in spite of 2D as well as electronic nature of diamane is considered isotropic. To ensure that Schottky junction has been formed at interface, the electric contacts have been made along the c-axis so that maximum charge carriers get collected. To obtain the high efficiency, various parameters of n-type diamane as well as p-type c-Si layers have been optimized and the maximum efficiency of 16.84% has been obtained for single layer n-diamane at 100 μm thick silicon wafer. We also investigated the spectral response and dependency of temperature on the performance of exclusively designed solar cell and we obtained the best efficiency 16.84% at 300 K temperature. In order to check the performance on commercially available silicon we have optimized the same solar cell by considering the parameters of commercially available p-type crystalline silicon layer and maximum efficiency 10.41% was achieved. After getting the maximum efficiency 16.84% we further carried out the simulation by optimizing the layer numbers of n-diamane and found decrement in the efficiency up to 15.3% which indicates that, efficiency slightly decreases as layer number increases. We have demonstrated that n-type diamane might be used as an effective emitter layer in crystalline Si heterojunction solar cell.

© 2022 The Authors. Published by Elsevier Ltd.
This is an open access article under the CC BY license (http://creativecommons.org/licenses/by/4.0/)

1. Introduction

Recently, a new allotrope of the carbon named as "Diamane" (Dn) possess sp^3 carbon bonding has been synthesized and reported to be two-dimensional (2D) being a physical analogue to "graphene-graphane" [1–4]. Recently, Bakharev et al. [5] confirmed that diamane exhibited 2 D electronic system. It was confirmed by estimating the optical band gap of diamane adopting the approach described in previous studies [6,7] for 2D electronic systems. They found that the experimental optical gap value of 3.3–3.4 eV is consistent with the calculated optical gap of 2.87 eV obtained for F-diamane. Furthermore, Raman spectroscopy was used to confirm the successful synthesis of 2D diamane and the characterization of its electronic structure has also been reported [8,9]. It has thermal conductivity of 1960 W/mK as high as to its bulk counterpart diamond (1000 W/mK), due to which it is considered as promising material for the high temperature electronic applications [1,10]. Furthermore, density functional theory (DFT) calculations reveal that 2D diamane has smaller effective mass ($0.55m_0$) of conduction electrons in comparison of its bulk counterpart i.e., diamond ($0.57m_0$), which is also very promising to use 2D diamane in various electronic applications such as solar cells [1]. 2D materials are best to use in electronic applications as they have large tunability in their bandgaps and they are flexible, strong and extremely thin. It was first predicted by Chernozatonskii et al., in 2009 [11], although its experimental synthesis was reported recently. The detailed verification of its bonding and electronic structure has also been probed by using various characterization techniques like: X-ray photoelectron spectroscopy (XPS), UV photoelectron, Raman, UV–Vis and electron energy loss spectroscopies, transmission electron microscopy and X-ray Diffraction (XRD) [5]. Formerly, the instability of diamane was marked as a big hurdle for its above-mentioned potential applications. Recently, the stability of diamane has been improved by the substitution of N atoms on its surface. The N atom has one more electron than C atom that form lone pair of electrons and behaves as the passivation, which stabilizes the structure and extends the band gap [2]. The first principal method has investigated the configuration

* Corresponding author.
E-mail address: pawantyagi@dtu.ac.in (P.K. Tyagi).

https://doi.org/10.1016/j.cartre.2022.100209
2667-0569/© 2022 The Authors. Published by Elsevier Ltd. This is an open access article under the CC BY license (http://creativecommons.org/licenses/by/4.0/)

stability and electronic properties of N-doped diamane [2]. This novel 2D material has direct band gaps which can be controlled in the range from 0.86 to 5.68 eV [4]. Furthermore, due to its large bandgap, the intrinsic carrier concentration stays low even at the high temperature. Furthermore, the substitution of N atoms makes these films highly n-type, and it is found that N-substituted diamanes are harder than fully hydrogenated diamanes [2]. Atomistic simulation demonstrated that diamane carries giant in plane stiffness (715 N/m) as compare of graphene (238 N/m) and graphane (449 N/m) [1,11]. It is noteworthy to mentioned that diamane possess high carriers' mobility, for electrons (2732 cm^2/Vs) and for holes (1565 cm^2/Vs) in case of fluorinated and hydrogenated diamane, which is superior over those of III-IV semiconductor compounds [12] and reported in 2 D materials. The calculated band gap for fluorinated diamane (C_4F) (2.93 eV) confirms its high transparency [13]. It has to be noticed that the work function of 2D diamane can also be turned in the range of 7.24 eV to 0.62 eV after vacuum annealing at 700 °C and the work function of as-grown bilayer graphene was reported to be 4.4 eV [14,5] which also opens up its use in various electronic applications. Above-mentioned unique properties of ultrathin 2D diamane film motivate us to explore the potential application of n-type diamane as an effective emitter layer in Si-based heterojunction photovoltaic cells. The role of emitter layer in the crystalline silicon heterojunction solar cell is not only to allow the maximum photons to surpass across the interface but also to develop a built-in potential at diamane/silicon interface which require to discrete the photogenerated charge carriers. In recent time, diamane is expected to be used in various areas such as nano-optics, nano-electronics, nano-electromechanical systems, mechanical resonators and electronic devices at high temperature [5]. In spite of that, the application of diamane in the solar cell has not been much investigated yet. This also inspired us to use n-type diamane as an emitter layer in the silicon heterojunction solar cell. As diamane layer number increases from one to five, there was a small decrement in the efficiency from 8 to 7.53%. Since, this small efficiency was not worthy to obtain an efficient solar cell therefore, it had become more necessary to optimize the values of parameters of p-cSi as well so that an affordable solar cell with less manufacturing cost can be achieved with better efficiency. Thus, in the present article, solar cell modeled as ITO (front contact)/n-Dn/p-cSi/Ag was optimized under the illumination of monochromatic light with a power density of 100 W/cm^2 and spectral width of 10 nm by using latest version 2.5 of the software AFORS-HET. This software generally solves the 1-D semiconductor equations such as continuity equation, transport and Poisson's equation for both holes and electrons by using finite difference at different conditions. In this simulated cell, the n-diamane has been chosen as an emitter layer or conducting electrode while, the p-cSi as an absorbing layer. The variables of both n-diamane and p-cSi layer were optimized to achieve the notable efficiency for n-diamane/p-cSi solar cell. The simulation was performed by considering the isotropic elastic nature of diamane layer. Since, diamane is isotropic in nature therefore the efficiency will remain same for both armchair and zig-zag direction in diamane layer. The purpose of this simulation is to analysis the impact of isotropic nature of diamane and silicon wafer on the functioning of solar cell and to enlighten the cell response.

2. Device structure and simulation details

The proposed structure of solar cell is shown in Fig. (1). To design this structure, we have used current version 2.5 of AFORS-HET (Automat FOR Simulation of Heterojunction) software which uses Shockley-Read-Hall recombination statistics for different layers of solar cell [15]. In the proposed structure of solar cell, ITO(TCO)/n-diamane/p-crystalline Silicon/Ag (back contact) displayed in Fig. (1). We have taken ITO as transparent conducting oxide (TCO) as well as anti-reflector to ensure that maximum number of photons get transmit. So, as the light incident on the cell photons get absorb in the absorber layer, as photon absorption increased in the active layer more electron and hole pairs will be generated. In this way, to achieve the maximum electron-hole pairs generation in the absorber layer we intend to use the material of highest transmission efficiency and to fulfill this purpose we used ITO as TCO. ITO can directly be deposited on diamane with the help of electron beam and pulsed layer deposition (PLD) technique transferred on SiO_2/Si pattern substrate [16–19]. Microstructure, surface morphology, electrical and optical properties of ITO film can be characterized and analysed by using various techniques like: XRD, scanning electron microscopy, atomic force microscopy, high resolution transmission electron microscopy. The standard transmission line model (TLM) method was used to evaluate sheet resistance ITO/n-Si contacts in HJ silicon solar cells [20]. This deposition technique might not be harmed the diamane as well as SiO_2/Si substrate. Ag was chosen as the back contact as shown in Fig. (1). The [n, k] file for front contact as well as back contact was taken as default which are in-built in the software. All the details about the parameters of front and back contacts are tabulated in Table 1. The proposed structure was illuminated under Air Mass 1.5 G, spectral width 10 nm with the power density of 100 mW/cm^2 as a light source. Simultaneously, the temperature of the cell was maintained at 300 K. Since, we prefer to take the reflection coefficient of front contact as smaller and the reflection coefficient of back contact as higher for getting higher efficiency. The front contact should be transparent ideally, so that maximum light can pass through the surface and get collected at the absorbing layer. Therefore, in this simulation we have taken the reflection coefficient of front contact as nearly zero whereas, the reflection coefficient of the back contact was taken as 0.05. The generation of electron-hole pairs was described by Lambert-Beer model which is in-built in the software and the reflection from the diamane/Si interface is not considered [15]. Shockley-Read-Hall recombination and/or dangling-bond recombination was considered as recombination model within the software including some defect states within the bandgap. ITO/n-Dn interface is considered as MS-Schottky front interface and the back interface i.e., p-cSi/Ag is also considered as MS-Schottky. To interpret the transportation of charge carriers in diamane layer, drift and diffusion model was applied in the software, where the differential transport equation for both holes and electrons was taken as 2-D in nature with carrier densities in A/cm [15]. At diamane/Si interface, two-dimensional equations are coupled with three-dimensional equations (as we know diamane is 2D and c-Silicon is 3D in nature) to act for the transport and boundary conditions at the interface. In this simulation, we have not assumed any mismatching of lattices between the layers and the movement of minority charge carriers has been considered through the c-axis. Ideally, diamane is 2-dimensional, only if this fulfils the condition $< t > \leq \lambda_F$, where <t> is average thickness of diamane, λ_F is the Fermi wavelength

Table 1
Information of the parameters used as front and back contact in the designed solar cell.

Contact variables	Front contact	Back contact
Material	ITO	Ag
Width (m)	8×10^{-8}	1×10^{-4}
File	ITO.nk	Ag. nk
Metal work function	Yes (flat band)	Yes (flat band)
Absorption loss	ITO. Abs	0
External reflection constant	0	0.05
Surface condition	Plane	Plane
Internal reflection constant	0	0

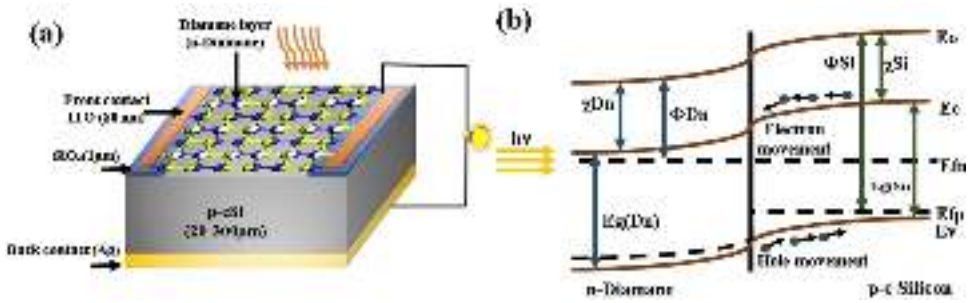

Fig. 1. (a) Schematic diagram of the simulated structure, (b) Schematic diagram under forward biasing just after the formation of heterojunction showing the transportation of electrons and holes. Φ_{Dn}, Φ_{Si} and χ_{Dn}, χ_{Si} are the diamane and Si work function and the diamane and silicon affinity, respectively.

Table 2
Ranges of other parameters chosen for the simulation.

Input parameters	Diamane	p-cSi
Thickness (cm)	0.3×10^{-7} – 1.5×10^{-7}	0.002–0.03
Dielectric constant (ε_r)	4–11	11.9
Electron affinity χ (eV)	3.3–5.2	3.6–4.5
Band gap, E_g (eV)	0.8–5.6	1.12
Optical band gap, E_g (eV)	2.8	1.124
Conduction band density, N_C (cm^{-3})	1×10^{19}–1×10^{21}	3×10^{19}–1×10^{21}
Valence band density, N_V (cm^{-3})	1×10^{19}–1×10^{21}	3×10^{19}–1×10^{21}
Electron mobility, μ_n (cm^2/Vs)	2732	1500
Hole mobility, μ_h (cm^2/Vs)	743–1565	500
Acceptor concentration N_A (cm^{-3})	0	1×10^{16} – 7×10^{18}
Donor concentration N_D (cm^{-3})	3×10^{14} – 1×10^{18}	0
Electron thermal velocity, V_e (cms^{-1})	3×10^7	1×10^7
Hole thermal velocity, V_h (cms^{-1})	3×10^7	1×10^7
Layer density, (gcm^{-1})	2.328	2.328
Auger electron recombination coefficient, (cm^6s^{-1})	0	0
Auger hole recombination coefficient, (cm^6s^{-1})	0	0
Band-to-band recombination coefficient, (cm^3s^{-1})	0	0
Defect properties	Single acceptor	Single acceptor
Total trap density (cm^{-3})	1×10^{14}	1×10^{14}
Characteristic energy (eV)	0.56	0.56

given as $\sqrt{\frac{2\pi}{n_{2D}}}$, and n_{2D} is the carrier density in cm^{-2}[21]. As diamane is synthesized by chemical exposure of bilayer graphene to H or F atoms which results in their attachment to graphene surface, hence we have taken the value of carrier density reported in graphene. By following the condition reported by Sarma et al. [22], even n~10^5 cm^{-3} in graphene cannot satisfy the above-mentioned condition additionally, it has also been reported that doping in 2D materials increases the interlayer spacing [21,23]. Therefore, we have considered both graphene as well as diamane as quasi 3D. The quantum confinement can be obtained by lowering the thickness. The thickness of single layer diamane is taken as 0.334 nm and the [n, k] file has been calculated by using the data provided in the previous literature [24]. The value of refractive index (n) and extinction coefficient (k) are estimated to be 1.5 and 2.7, respectively [24]. Because of isotropic nature of diamane, properties like mobility and effective mass of charge carriers are same in both armchair and zigzag directions.

For optimizing the cell parameters and to simulate the cell, the bulk and interfacial defect distribution as well as recombination rate (G) were taken constant in the software. Moreover, the model chosen for ITO/n-diamane and p-crystalline Si/Ag interface was MS-Schottky model and the model chosen for n-diamane/p-cSi interface is drift-diffusion, respectively. The parameters which have to be optimized are: N_D (donor concentration), N_C/N_V (effective conduction and valance band density), energy bandgap (E_g), χ (affinity), ε_r (dielectric constant), layer thickness, electron and hole mobilities (μ_n, μ_h). The optimization of above-mentioned parameters for diamane was carried out by taking the set values of parameters of p-cSi layer in the range of reported values in the literature and have been tabulated in Table 2. N_C/N_V of diamane have been calculated by using the equation as follows:

$$N_{C/V} = 2\left(\frac{2\pi k_B T m^*_{e/h}}{h^2}\right)^{\frac{3}{2}} \quad (1)$$

Where k_B is the Boltzmann constant, T is the temperature in Kelvin, m^*_h is the hole effective mass, m^*_e is the electron effective mass and h is the Planck's constant [25,26]. Whereas, the thermal velocity (V_{th}) of charge carriers has been calculated by using the relation $V_{th} = \sqrt{\frac{3k_BT}{m^*_{e/h}}}$. After getting the best optimized results of diamane's parameters, we have further optimized the various parameters of p-type c-Si wafer such as: N_A (acceptor concentration), N_C/N_V (conduction band and valance band density), χ (affinity), and wafer thickness by keeping the parameters of n-Dn at their best optimized values. The range of parameters of n-diamane have been taken from the available literatures [4,12,14,16,21,26] and the range of parameters of p-cSi which we have considered here are for (100) oriented single crystalline Si [26–29] tabulated in Table 2.

The schematic of energy band diagram for the proposed structure ITO (TCO)/n-Dn/p-cSi/Ag has been depicted in Fig. 1(b). Since, drift-diffusion effect is considered at the interface therefore, the majority of charge carriers i.e., electrons from the n-diamane and holes from the p-cSi are diffused towards each other until thermal equilibrium is developed. This happens because of concentration gradient at the interface, this phenomenon is called diffusion process. An electric field exists in the depletion region which spread up to some width called depletion width W, in both p and n regions. Both electrons and holes in this depletion region are carried away by this electric field. As a result, a drift current devel-

ops which balances the diffusion current and appears due to the difference in electron and hole densities at the junction. As a result, thermal equilibrium is established and the energy bands start bending near the Fermi level. The built-in potential (eV_{bi}) is the reason for charge segregation across the junction in the solar cell as discussed above. This built-in potential (eV_{bi}) in both p-cSi and n-diamane can be framed in the form of work-function according to the equations written as follows:

$$e.V_{bi} = \Phi_{BI} = \Phi_{Si-P-type} - \Phi_{Dn,\ N-type}$$

$$= -\chi_{Dn} - kT \ln\left(\frac{N_C}{N_D}\right) + \chi_{Si} + kT \ln\left(\frac{N_A}{N_V}\right) \quad (2)$$

Where Φ_{Dn} and Φ_{Si} are the work function of diamane and silicon, respectively. Whereas, χ_{Dn} and χ_{Si} are the affinity of diamane and Si, respectively. Moreover, N_D is the donor concentration and N_C is the effective conduction band density for diamane, while N_A is acceptor concentration and N_V is the effective valence band density for p-crystalline Si [26,30].

As n-diamane/p-crystalline Si junction is illuminated, it gives rise to electron-hole pairs (EHP) which gets separated because of the built-in potential. The minority charge carriers flow towards the n-diamane and p-crystalline Si respectively, depicted in Fig. 1(b). When open circuit condition is applied, the photo-generated charge carriers intensify the carrier density in their corresponding fields and because of this intensification of charge carriers, quasi-Fermi level approaches the conduction band in n-diamane and valance band in p-cSi as a result V_{OC} develops. In the same manner under short-circuit condition, these photo-generated charge carriers do not intensify because of the collection of charge carriers at their respective electrodes which results in the J_{SC} that flows in the outer circuit.

3. Results

3.1. Optimization of n-type diamane layer parameters

To simulate the above designed cell, first we have optimized the doping concentration (N_D) of n-type diamane layer ranging from 3×10^{14} cm^{-3} to 1×10^{18} cm^{-3} while keeping other parameters of diamane and p-type c-silicon at some reasonable values reported in the literatures [4,12,14,16,21,26–29] and the results obtained from this optimization have been plotted in Fig. 2 (a and b). Fig. 2 (b) shows that, as N_D increased from 3×10^{14} cm^{-3} to 1×10^{18} cm^{-3}, V_{OC} found to be constant at 521.1 mV. It might be happened because as we increase the doping concentration above 3×10^{14} cm^{-3}, mobility decreases due to enhance collisions of charge carriers with ionized doping atoms which results in decrease of carrier's lifetime according to the relation: $\mu_i = \frac{e}{m^*}\tau_i$ here, e is the electronic charge and m^* is the effective mass of electron. Since, mobility and diffusion constant relate by Einstein's relation given by $\frac{D_i}{\mu_i} = \frac{k_B}{e}T$ [25,26] and indicates that as mobility decreases diffusion constant also decreases as it is directly proportional to the mobility of charge carriers and therefore, diffusion length ($L_i = \sqrt{D_i \tau_i}$) reduces. Diffusion length is the average distance an electron can move and recombine, it depends on the recombination time as well as diffusion constant. In this manner, J_{SC} will also decrease and J_0 increases following the relations given below:

$$J_{SC} = qG(L_n + L_p) \quad (3)$$

Where L_n and L_p are the diffusion length of electron and hole, respectively. q is the electric charge and G is the electron and hole pair generation rate [26,31].

$$J_0 = eA\left(\frac{D_p P_n}{L_n} + \frac{D_n n_p}{L_p}\right) \quad (4)$$

Where, A is the area of junction [25,26]. This increment in J_0 and decrement in J_{SC} results in a reduction of V_{OC} following by the relation:

$$V_{OC} = \frac{nqT}{k} ln\left(\frac{J_{SC}}{J_0} + 1\right) \quad (5)$$

here, J_0 is the reverse saturation current. But at the same time, V_{bi} increases according to Eq. (2), results in higher V_{OC}. These two processes contradict each other and make the balance to keep V_{OC} at a constant value 521.1 mV. Another possibility for V_{OC} being constant at 521.1 mV is that V_{OC} is independent of N_D, if it satisfies the condition: $\Delta\ n_o >> N_D$, where $\Delta\ n_o$ is the additional electron and hole pairs [26,32]. Further, as we increase N_D from 3×10^{14} cm^{-3} to 5×10^{15} cm^{-3}, the conductivity of diamane layer was found to increase and consequently, J_{SC} increased very slightly from 20.87 to 20.99 mA/cm^2. On further increasing N_D from 5×10^{15} cm^{-3} to 1×10^{18} cm^{-3}, J_{SC} start decreasing from 20.99 to 20.67 mA/cm^2, this happens because at higher N_D, diffusion length decreases and as a result J_{SC} decreases. Another reason behind this decrement in the value of J_{SC} from 20.99 to 20.67 mA/cm^2 after N_D 5×10^{15} cm^{-3} is that on increasing doping concentration, work function will reduce due to this reduction in work function J_{SC} falls off. From Fig. 2(a) it is observed that there is a sudden increase in the value of fill factor (FF) and efficiency (η) after $N_D = 3 \times 10^{14}$ cm^{-3}. This might be happened because of the decrement in the sheet resistance which reduced on increasing doping concentration. After $N_D = 1 \times 10^{16}$ cm^{-3}, FF and η decrease very slightly and then again starts to increase as N_D increases. Maximum efficiency 7.74% was achieved at $N_D = 10^{18}$ cm^{-3}. Therefore, the best optimized value of N_D for n-type diamane layer found to be 1×10^{18} cm^{-3}.

After optimizing N_D at 10^{18} cm^{-3}, the next parameter conduction/valence band density (N_C/N_V) is optimized by varying in the range of 1×10^{19} cm^{-3} to 6×10^{21} cm^{-3} for ultra-single diamane wafer. On increasing N_C/N_V, the densities of minority charge carriers get reduced. This reduction in minority carriers is possibly because of the smaller period of photo-generated carriers and trapping of the free charge carriers. Due to which, V_{OC} will remain constant at 521.1 mV as we varied N_C/N_V from 1×10^{19} cm^{-3} to 6×10^{21} cm^{-3}. From the Fig. 2(c, d), we noticed that J_{SC} increases linearly on increasing N_C/N_V of diamane layer this increment in J_{SC} is due to the high value of N_C which leads to higher absorption of photons. It is also observed that the FF reduces linearly from 71.88% to 65.12% on varying the N_C/N_V from 1×10^{19} cm^{-3} to 6×10^{21} cm^{-3}. Since FF is reducing consequently, η will be reduced from 7.74% to 7.04%. Maximum efficiency 7.74% was achieved at $N_C/N_V = 1 \times 10^{19}$ cm^{-3}. Hence, 1×10^{19} cm^{-3} is the best optimized value of N_C/N_V for single layer n-diamane.

After optimizing N_D and N_C/N_V, the next parameter bandgap (E_g) is optimized in the range of 0.86 to 5.6 eV. Here, we have chosen a higher range of bandgap for the simulation by keeping in mind that if the UV light present in solar light could contribute to the higher bandgap. We have taken this range of bandgap in order to see the effect of bandgap on the solar cell's efficiency for all derivatives of diamane as it has various derivatives which possesses a range of bandgap depending on the functional group they contain and many other factors too. But we did not notice any change in the efficiency of solar cell after the bandgap 1.3 eV. It is reported that dielectric constant is inversely proportional to the bandgap energy therefore, on changing the bandgap value dielectric constant also changes. For higher bandgap dielectric constant becomes smaller which consequently increases the recombination loses due to the improvement in the exciton binding energy. Therefore, on further increasing the bandgap there will not be seen any improvement in the value of efficiency of the solar cell and it became constant 7.74% after the bandgap 1.3 eV. In this specific sec-

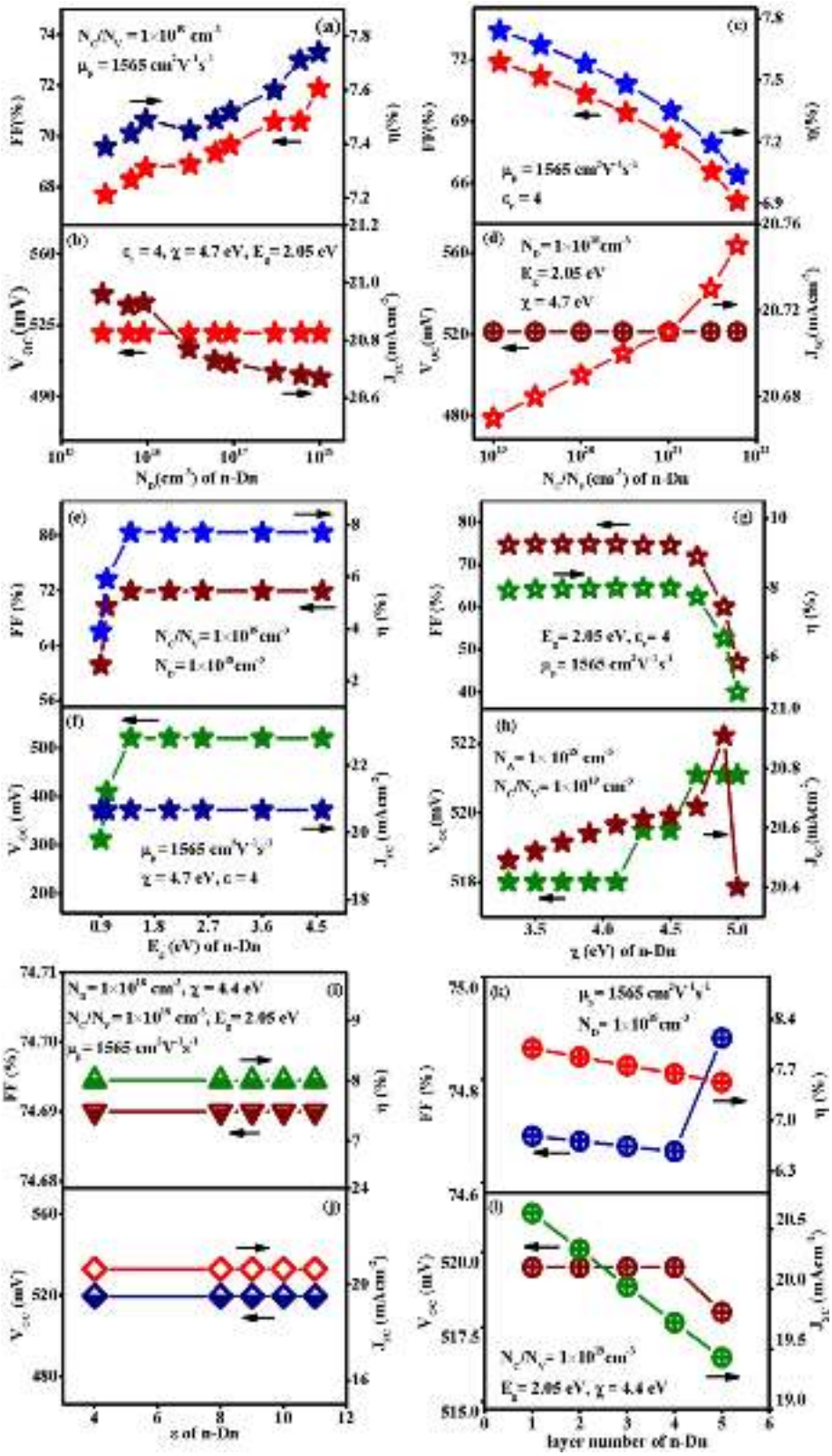

Fig. 2. Graphic representation of the performance of designed cell after optimization of different variables of n-diamane, (a, b) N_D (cm^{-3}) donor concentration, (c, d) N_C/N_V (cm^{-3}) effective conduction/valance band density, (e, f) bandgap E_g (eV), (g, h) χ (eV) electron affinity, (i, j) dielectric constant ε_r, and (k, l) layer numbers. After fixing the variables of p-cSi at some constant values like: N_A (acceptor concentration) = 1 × 10^{16} cm^{-3}, N_C/N_V (effective conduction/valance band density) = 3 × 10^{19} cm^{-3}, χ (affinity) = 4.05 eV and layer thickness = 100 μm. Remaining variables of both p-cSi and n-Dn are mentioned in Table 2.

tion of manuscript, we discussed only about the effect of varying the bandgap because we exclusively want to see the effect of varying bandgap on the performance of solar cell. Therefore, we did not discuss about the variation in the dielectric constant here. We have discussed about the effect of varying the dielectric constant on the performance of solar cell in another section of the manuscript. As we increased E_g, V_{OC} found to be increased and attained a constant value 521.1 mV at 1.3 eV. Whereas, J_{SC} remains constant at 20.67 mA/cm^2 as depicted in Fig. 2(f). In Fig. 2(e), it has been shown that FF and η increase from 63.96% to 72.09% and 2.79% to 7.74% respectively, for the bandgap ranging from 0.86 to 1.25 eV and then attain a constant value 71.88% for the FF and 7.743% for the efficiency at the bandgap 1.3 eV. Therefore, the bandgap 1.3 eV is the best optimized bandgap for single layer n-diamane.

The optimized results of the electron affinity (χ) in the range from 3.3 eV to 5.2 eV is shown in Fig. 2 (g and h). As χ increased, very slight increment in the value of η from 7.92 to 8% was observed up to the electron affinity 4.4 eV and then a dramatical reduction in the value of efficiency was noticed as shown in Fig. 2(g). The reason behind this small linear increment in the efficiency is that as we increase electron affinity of single layer diamane above 3.3 eV, the barrier height gets decrease which results in the fast movement of minority charge carriers as a result, J_{SC} increased. Thus, η was observed to increase linearly up to 4.4 eV. After 4.4 eV, as we increase affinity, the conduction band lowers down and starts making rapid transportation of charge carriers across the interface as a result, there would not be any free charge carrier. Consequently, J_{SC} and FF will be decreased which cause final η to decrease. Here, we found that on increasing χ, V_{OC} was improved and attained maximum value 524.2 mV at $\chi = 5.2$ eV and maximum η 8% was observed for $\chi = 4.4$ eV. Thus, 4.4 eV is the best optimized value of electron affinity for single layer n-type diamane.

After this we have optimized the value of relative permittivity (ε_r) or dielectric constant. The value of dielectric constant (ε_r) for a bilayer graphene was found to be in the range from 4 to 9 in different experiments [33]. Here we varied the value of relative permittivity (ε_r) in the range from 4 to 11 and the performance of proposed solar cell are depicted in Fig. 2 (i and j). From Fig. 2 (i and j), it is noticed that as the dielectric constant increased from 4 to 5 then may be due to the reduction in the excitation binding energy the recombination losses decreased and therefore the efficiency increased by a small value from 8.006% to 8.007%. But on further increasing the value of dielectric constant the efficiency falls off from 8.007% to 8.006% rather than increasing, as we know higher dielectric constant reduces the exciton binding energy which consequently results in decreased recombination losses. This may be have happened because it is reported that $V_{bi} \propto \frac{1}{\varepsilon_r}$ [25,26,34]. Therefore, an increment in the value of dielectric constant deteriorates V_{bi} which consequently decrease the efficiency [26]. In this manner, these two effects balance each other and no further change in the values of V_{OC}, J_{SC}, FF and η has been observed. In this way, the maximum efficiency 8.007% was achieved at the value 5 of dielectric constant.

After optimizing the relative permittivity (ε_r), we have further optimized the hole mobility of n-Dn layer ranging from 743 to 1565 cm^{2}V^{-1}s^{-1} and we noticed that there is no effect of hole mobility on the performance of the photovoltaic cell, because of the ultra-thin layer of diamane.

To understand the role of layers number of n-diamane in the production of charge carriers due to absorption of photons from sunlight by the solar cell with all parameters those we have optimized above at single layer diamane, the above simulated cell was further optimized up to 5 layers of diamane while keeping the parameters of c-Si at the previous constant values that we have taken for previous simulation. It is reported that as layer number increases, both sheet resistance as well as transmittance decrease which results in lowering the electron-hole pair generation rate at the interface that depends on the transmittance of diamane. We found that, as layer numbers of n-diamane increased, V_{OC} decreased very slightly from 519.5 mV to 518 mV and a variation in the value of J_{SC} was found from 20.63 mA/cm^2 to 19.14 mA/cm^2. This was happened, because of smaller electron-hole pair generation rate. The FF was also found to decreased slightly from 74.69% to 74.66% and then decreased infinitesimally on further increasing the number of layers. Because of lower value of V_{OC}, J_{SC} and FF, η also decreased from 7.88% to 7.53%. The best optimized efficiency 8% was achieved for single layer n-diamane. Since, we found deterioration in the values of V_{OC}, J_{SC}, FF and η on increasing the layer numbers of n-diamane we can say that thickness of n-diamane does not play an important role in improving the efficiency of the solar cell and the generation of photo carriers. We also know that on increasing the thickness the bandgap decreases which in results increases the dielectric constant which consequently decrease the recombination losses due to decrease in exciton binding energy. Therefore, according to this concept efficiency should get increased on increasing the thickness of n-diamane but this is not seen from the results shown in Fig. 2 (k and l). This may have happened because of the reduction in transmittance on increasing the layer number which compensates the effect of reduced bandgap on increasing the dimensionality of carbon material (diamane). From Fig. 2 (k and l) it is noticed that on increasing the layer number of diamane from 1 to 5 the efficiency changed slightly from 8% to 7.53%. Therefore, we can say that increased number of layers of diamane do not play a significant role in enhancing the efficiency of solar cell. It only provides the required Schottky junction at the interface for the current movement and act as an effective emitter layer in c-Si heterojunction solar cell.

3.2. Optimization and simulation of p-crystalline silicon wafer parameters

We further optimized variables of p-crystalline Si wafer while, setting the parameters of n-Dn at best optimized values. To carry out this simulation, first we optimized the acceptor concentration of p-cSi wafer. This will intensify the efficiency of the ITO (TCO)/n-Dn/p-cSi/Ag structured solar cell, the value of N_A for p-cSi wafer was increased from 1×10^{16} cm^{-3} to 7×10^{18} cm^{-3} and the desired outputs are shown in Fig. 3 (a and b). As we increase N_A, the Fermi Level in Si layer moves towards the valence band edge and results in an increase of work function of p-type Si (Φ_{p-Si}), and barrier height according to Eq. (2) which will increase both V_{bi} and V_{OC} according to the equations:

$$V_{OC} = \frac{V_{bi}}{q} - \frac{nkT}{q} \ln\left(\frac{qN_V S_{it}}{J_{SC}}\right) \quad (6)$$

$$V_{bi} = \frac{kT}{q} \ln\left(\frac{N_A N_D}{n_i^2}\right) \quad (7)$$

Where, S_{it} is the interface recombination velocity [35–37]. Therefore, as N_A increases V_{bi} also increases which helps the generated charge carriers in approaching their respective electrodes due to which the values of both V_{OC} and J_{SC} enhanced from 519.5 mV to 697.7 mV and 20.63 mAcm^{-2} to 28.71 mAcm^{-2} respectively, as depicted in Fig. 3(b). FF and η were also noticed to increase with N_A from 74.69% to 83.58% and from 8% to 16.74% respectively, as shown in Fig. 3(a). The increment in FF might be related to the decrement in the resistivity of the p-cSi layer [26,38]. The maximum efficiency 16.74% was achieved at $N_A = 7 \times 10^{18}$ cm^{-3}. Therefore, 7×10^{18} cm^{-3} is the best optimized value of N_A for p-cSi layer Eqs. (6), (7).

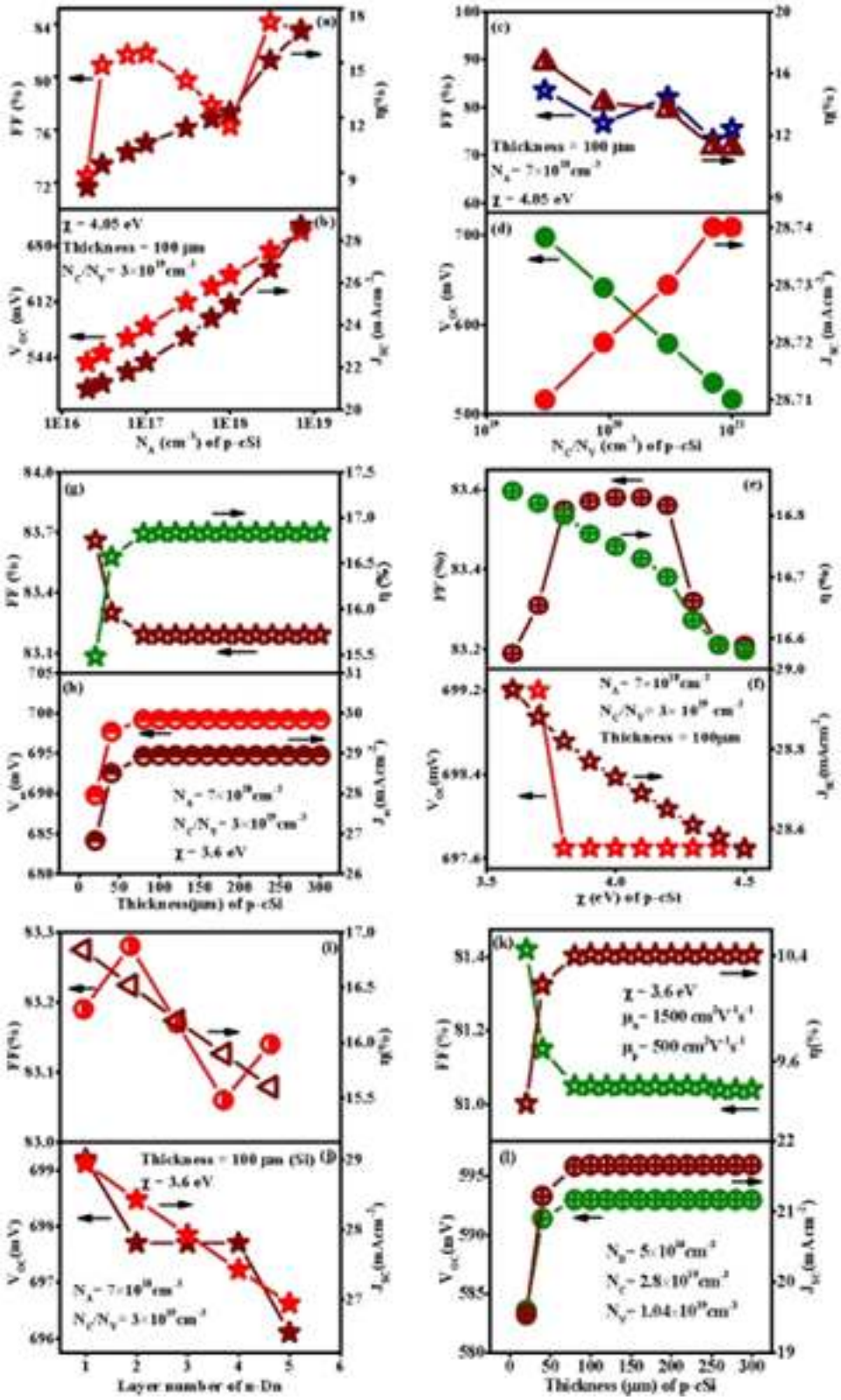

Fig. 3. Graphic representation of the performance of the designed cell after simulation of different variables of p-crystalline Si wafer, (a, b) acceptor concentration N_A (cm^{-3}), (c, d) N_C /N_V (cm^{-3}) conduction/valance band density, (e-f) χ (eV) affinity, (g, h) wafer thickness (μm), (i, j) layer number of n-Dn at best optimized values of p-cSi wafer and (k, l) thickness of Si layer at commercially available values of parameters p-cSi wafer, whereas the values of parameters of n-Dn are kept at their best optimized values i.e., $N_D = 1 \times 10\ 18$ (cm^{-3}), $N_C/N_V = 1 \times 10\ 19$ (cm^{-3}), $E_g = 2.05$ (eV), $\chi = 4.4$ (eV), $\mu_n = 2732$ ($cm^2V^{-1}s^{-1}$) and $\mu_p = 1565$ ($cm^2V^{-1}s^{-1}$).

After getting best optimized value of N_A, we carried out the simulation further by optimizing N_C/N_V of p-cSi ranging from 3×10^{19} cm^{-3} to 1×10^{21} cm^{-3} and the outputs are plotted in Fig. 3 (c, d). Here we found that the V_{OC} is decreased from 697.7 mV to 516.4 mV as N_C/N_V increased. As N_C/N_V increases, V_{bi} increases by following Eq. (2). Therefore, the trapping speed of charge carriers inside the Si layer reduce. On more increasing the value of N_C/N_V, the mobility and L_i of charge carriers decrease by following the Eqs. (1), (3) and (4). By taking the Eq. (5) in consideration we can say that J_O also increases on increasing N_C/N_V. This increment in the value of J_O as well as V_{bi} results in the decrement of V_{OC}. The value of J_{SC} was found to increased very slightly from 28.71 $mAcm^{-2}$ to 28.74 $mAcm^{-2}$ as we increased N_C/N_V of p-cSi from 3×10^{19} cm^{-3} to 5×10^{20} cm^{-3} and then becomes constant. This might have happened because, the bandgap and photons absorption are highly influenced by N_C/N_V [26,39]. Therefore, at $N_C/N_V = 3 \times 10^{19}$ cm^{-3}, active silicon layer absorbed more photons which increased the generation rate (G) of electron-hole pair (EHP) and then according to Eq. (3), the higher value of G may balance the lower value of L_i which results in constant value of J_{SC} 28.74 $mAcm^{-2}$. The FF was first found to increase slightly from 83.58 to 83.63% and then decreases up to 75.58% on further increasing the value of N_C/N_V after 8×10^{19}. The efficiency was found to be decreased linearly from 16.74% to 11.22% on increasing N_C/N_V from 3×10^{19} cm^{-3} to 1×10^{21} cm^{-3} as depicted in Fig. 3(c). The initial increment in FF may be because of an increment in J_{SC}. At higher value of N_V, FF decreases abruptly because it depends on V_{OC}. In the similar manner, a direct decrement in the value of η was observed because of its direct dependency on FF. The maximum value of efficiency 16.74% was found at $N_C/N_V = 3 \times 10^{19}$ cm^{-3}. So, 3×10^{19} cm^{-3} is the best optimized value of N_C/N_V for p-cSi layer.

After optimizing N_A and N_C/N_V to their best optimized values we further optimized the electron affinity of p-cSi layer in the range from 3.6 to 4.5 eV. For this affinity, V_{OC} was found to slightly increased from 699.2 mV to 697.7 mV on increasing affinity from 3.6 eV to 3.8 eV and then it stayed constant at the value 697.7 mV on further increase in affinity after 3.8 eV. Whereas, the value of J_{SC} was noticed to decrease straight from 28.95 mA/cm^2 to 28.55 mA/cm^2 as depicted in Fig. 3(e, f). The value of FF first increased from 83.19% to 83.58% on increasing the electron affinity from 3.6 eV to 4.1 eV but on further crossing of the value of electron affinity the FF starts decreasing from 83.58% and reached 83.21% at affinity 4.5 eV. This reduction in FF on increasing the affinity from 4.2 eV to 4.5 eV can be understood by the concept of changing the work function of p-cSi at the interface by the relation: $\Phi_B = \Phi_{p-cSi} - \chi$, where Φ_B is the barrier height for p-type semiconductor, Φ_{p-cSi} is the work function of p-cSi and χ is the affinity of Si due to which the carrier transportation rate in the p-cSi layer would reduce. This reduction will increase the series resistance of both p-cSi wafer and the cell. Therefore, the FF reduces after $\chi > 4.1$ eV. The efficiency of the optimized cell was found to decrease linearly from 16.84% to 16.58% as we increase affinity in the range 3.6 to 4.5 eV. In this way the best optimized cell was obtained at affinity 3.6 eV.

To further analyze the possibility of cost-effective cell, the next variable we optimized is the thickness of p-cSi layer. We have optimized the thickness of p-cSi wafer ranging from 20 to 300 µm. From Fig. 3 (g, h), it is clearly visible that for 20 µm thick p-cSi layer, the efficiency is 15.48%. Higher efficiency 16.84% was obtained for 100 µm thick silicon layer. This is because as the thickness increases number of charge carriers increases consequently, J_{SC} increases. For thicker layer of p-cSi, the lifespan of minority charge carriers gets reduced because of its less drift length. Additionally, the excess photogenerated charge carriers and their recombination rate have been found in proportion in the thicker silicon wafer, which overall results in a constant value of V_{OC} 699.2 mV and J_{SC} 28.95 $mAcm^{-2}$ after thickness 100 µm. The FF and efficiency were also constant after getting a value 83.19% and 16.84% respectively, beyond the thickness 100 µm. Thus, we did not notice any change in the value of V_{OC}, J_{SC}, FF and η on further increasing the thickness of p-cSi layer after 100 µm and we can say that, these saturated values of V_{OC}, J_{SC} and FF have produced a maximum efficiency of 16.84%, even on increasing the thickness of p-cSi wafer up to 300 µm. Another reason for not improving the efficiency further on increasing the thickness of p-cSi wafer beyond 100 µm is that in a thick layer of p-cSi more dangling bonds is found which became the recombination centers for the photogenerated charge carriers due to the increased number of defects on the surface of thick silicon layer. That is why, the decreased bandgap on increasing the thickness of layer does not contribute in improving the conversion efficiency of the solar cell. Therefore, large thickness of p-cSi does not find to play an important role in improving the efficiency of the cell. From Fig. 3 (g and h) it is shown that during the optimization of thickness of p-cSi layer the efficiency increases from 15.48 to 16.84% only which is not much recommendable.

After optimization of silicon wafer's parameters, the cell was further simulated to studied the effect of the layer numbers of diamane and the results are plotted in Fig. 3 (i and j), where we found η to decrease from 16.84% to 15.6%. For best commercial appreciation of the simulated cell, we have further optimized the thickness of p-cSi wafer by considering the commercially available parameters of Si layer. For this, we have taken the values of acceptor concentration = 5×10^{16} cm^{-3}, effective conduction band density = 2.8×10^{19} cm^{-3}, effective valance band density = 1.04×10^{19} cm^{-3}, affinity = 3.6 eV, electron mobility = 1500 cm^2/Vs and hole mobility = 500 cm^2/Vs from the previously reported data [26,40,41]. We optimized the thickness of silicon layer in the range from 20 to 300 µm and the highest efficiency 10.41% was found for thickness 100 µm as shown in Fig. 3 (k and l). Since, front and back contacts play an important role in the solar cell as the front contact is required to be highly transparent so that maximum photons can reach to the active layer and enhance the conversion efficiency. Therefore, we preferred the front contact with low reflection coefficient or nearly 0. Hence, we have given more preference to ITO (Indium Tin Oxide), as TCO (Transparent Conducting Oxide) in designing of our solar cell to intensify the effective illuminating area, because ITO increases the optical absorption instead of reflection that occurred in other metal contacts and it possesses low sheet resistance, high mobility and it is optically transparent too. Furthermore, in order to check the effect of back contact on the solar cell we have changed the back contacts by Au (where n is taken as 0.27049 and k is taken as 2.7789) and Tin (where n is taken as 1.96 and k is equal to 3.06), these files are present already in the AFORS-HET software and we found that maximum efficiency is achieved in case of Au and Ag because of their larger work function. This indicates that both reflection coefficient and work function of front as well as back constant play significant role in the solar cells. Here, we have given more preference to ITO (Indium Tin Oxide), as TCO (Transparent Conducting Oxide) in designing of our solar cell to intensify the effective illuminating area, because TCO increases the optical absorption instead of reflection that occurred in other metal contacts.

3.3. Spectral response, quantum efficiency and temperature dependency

Generally, spectral response is conceptually similar to the quantum efficiency (QE) of the solar cell**.** The QE is defined as the ratio of the number of electrons collected by the cell as output to the number of photons incident on its surface whereas, spectral re-

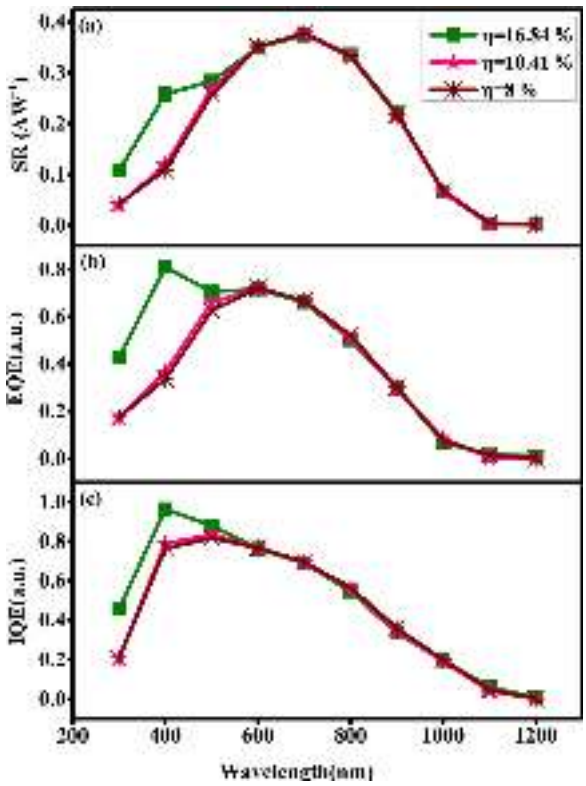

Fig. 4. Wavelength dependency of (a) SR (Spectral response), (b) EQE (External quantum efficiency) and (c) IQE (Internal quantum efficiency) of the best simulated solar cell at single layer n-Dn/p-cSi (η = 8%, η = 16.84% with $N_A = 7 \times 10^{18}$ (cm^{-3}), $N_C/N_V = 1 \times 10^{19}$ (cm^{-3}) for 100 μm p-cSi and efficiency = 10.41% with $N_A = 5 \times 10^{16}$ (cm^{-3}), $N_V = 1.04 \times 10^{19}$ (cm^{-3}) and $N_C = 2.8 \times 10^{19}$ (cm^{-3}) at 100 μm p-crystalline Si).

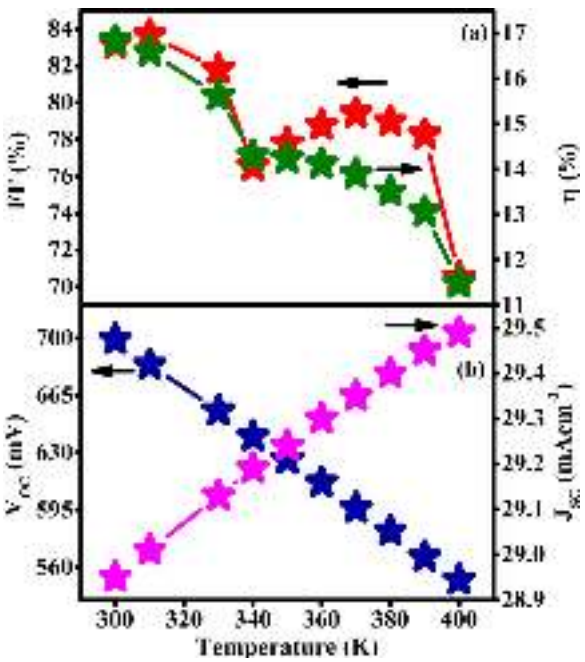

Fig. 5. Dependency of the optimized cell response with temperature variation at η = 16.84%. (a) efficiency and fill factor, (b) V_{OC} and J_{SC}.

sponse is defined as the ratio of current generated by the cell to the optical power incident on its surface [26]. Quantum efficiency and spectral response both are used in cell analysis one uses the photons flux and the other uses the power of light at each wavelength, respectively. QE can be converted into spectral response (SR) by using the formula: SR = $\frac{q\lambda}{hc}$ QE. To analysis the spectral response (SR), external quantum efficiency (EQE) and internal quantum efficiency (IQE) of the optimized cell at efficiencies 8%, 10.41% and 16.84% we performed the simulation in the wavelength range 300–1200 nm and the results are shown in Fig. 4. We observed that, at shorter wavelengths i.e., below 600 nm the diamane layer was found to absorb most of the light, this results in less photons passing to p-cSi layer subsequently small amount of current would generate in the shorter wavelengths and the cell response was found to be very low. In the wavelength range from 600 to 1000 nm most of the photons reach silicon layer where, the energy they constitute found equal to the bandgap energy of silicon layer and this energy then converted into electrical energy inside the silicon layer. Therefore, the optimized cell achieved its ideal response at intermediate wavelengths. Since silicon is an indirect bandgap semiconductor therefore, there will not be any sharp cut off at the wavelength corresponding to its bandgap (E_g= 1.12 eV). So, the spectral response falls back to zero at longer wavelengths. From Fig. 4, it is clearly visible that for greater than 100 µm thick silicon layer, spectral response maintained its uniformity. This is because the effective conversion rate remains constant as we increase thickness beyond 100 µm.

The internal and external quantum efficiencies (IQE and EQE) of the optimized cell at efficiencies 8%, 10.41% and 16.84% has been observed and the results are being shown in Fig. 4. Internal quantum efficiency do not consider the reflection and transmission of photon outside the solar cell while, EQE considers the outcomes of optical losses i.e., reflection and transmission. Fig. 4 (b and c) reveals that, at initial wavelength 300 nm EQE and IQE is having smaller value this is because of the optical losses at the shorter wavelengths. The IQE and EQE are maximum at the wavelength 400 nm and above 400 nm both efficiencies start falling off and reaches to zero at 1200 nm. Since, parameter's optimization of silicon as well as diamane was unable to nullify the optical losses on the surface of the solar cell. Hence, maximum EQE and IQE was noticed for the wavelength 400 nm. The higher value of EQE at the wavelength 400 nm suggests that as we optimize doping concentration and effective band density then there would be an increment in the electron-hole pair generation rate and subsequently, collection of surplus charge carriers due to which highest efficiency has been achieved at 400 nm. We found that, IQE and EQE responses of the cell with efficiencies 8%, 10.41% and 16.84% are almost same, which indicates the equal amount of charge carriers gathered for this range of wavelengths parallel to the photons absorbed by the solar cell. At higher wavelength regions, the recombination rate of the generated charge carriers is better therefore, both internal and external efficiencies become negligible at 1200 nm wavelength.

In order to realize the effect of varying temperature on the operation of solar cell we have further simulated the best optimized cell comprises efficiency 16.84% in the environment of 300 to 400 K temperature and the outputs are depicted in Fig. 5 (a, b). We observed that, V_{OC} decreased from 699.2 mV to 552.3 mV while, J_{SC} increased moderately from 28.95 mA/cm^2 to 29.49 mA/cm^2 as we increase the temperature. Following to Energy-Temperature relation written as: E_g (T) = E_g (0) – ($\frac{\alpha T^2}{\alpha+\beta}$), where E_g (T) is the bandgap of semiconductor at any given temperature T, E_g (0) is the bandgap at zero temperature and (α, β) are the material constant [26,31]. As temperature elevates band gap declines smoothly. We also know that, as temperature increases J_O increases which results in a decrease of V_{OC} [26,31]. Furthermore, at smaller value of E_g large number of absorbed photons have sufficient energy to create e-h pairs which results in an increment in the value of J_{SC}. Since

Table 3
Overview of the variables of the finest simulated solar cell.

Cell variables	n-diamane layer optimized cell	n-diamane layer and p-cSi layer optimized cell	p-cSi layer optimized cell for practically available Si parameters
V_{OC} (mV)	519.5	699.2	593
J_{SC} (mAcm^{-2})	20.63	28.95	21.66
FF (%)	74.69	83.19	81.05
η (%)	8 (@ p-crystalline Si wafer at $N_A = 1 \times 10^{16}$ (cm^{-3}), $N_C/N_V = 3 \times 10^{19}$ (cm^{-3}), $\chi = 4.05$ (eV), and thickness = 100 μm	16.84 (@ p-crystalline Si wafer at $N_A = 7 \times 10^{18}$ (cm^{-3}), $N_C/N_V = 3 \times 10^{19}$ (cm^{-3}), $\chi = 3.6$ (eV), and thickness = 100 μm	10.41 [@ p-cSi wafer at $N_A = 5 \times 10^{16}$ (cm^{-3}), $N_C = 2.8 \times 10^{19}$ (cm^{-3}), $N_V = 1.04 \times 10^{19}$ (cm^{-3}), $\chi = 3.6$ (eV), and thickness = 100 μm]

V_{OC} decreases, the fill factor and efficiency also decrease and the maximum efficiency $\eta = 16.84\%$ found at temperature 300 K. The optimized results of the designed solar cell are shown in Table 3.

4. Conclusions

In this article, we have proposed the structure (TCO) ITO/n-Dn/p-cSi/ (back contact) Ag. The independent consequences of optimizing seven parameters of n-type diamane wafer on the operation of solar cell were investigated and only single parameter: hole mobility (μ_p) was noticed to not influence its working whereas, other parameters were directly affecting the behavior of proposed cell. After optimizing the parameters of diamane as well as silicon, the maximum efficiency of 16.84% was achieved and the formation of Schottky junction at n-Dn/p-cSi interface was found to play major role in the processing of the cell as it helps in carrying current across the junction. This junction is responsible for the current movement across n-Dn/p-cSi interface. As the work function of diamane can be varied in the range 7.24 eV to 0.62 eV and the work function of p-type silicon layer is found in the range 4.9–5.1 eV. Here, we have taken the work function of diamane as 4.4 eV smaller than the work-function of p-type silicon which supports the formation of Schottky junction at the interface. We also compared the optimized values with the reported experimental values and found satisfactory results. Higher thickness of both diamane as well as silicon were not found to contribute in improving the efficiency of the solar cell on the large scale. It has been found that the thickness of front and back contacts does not play an important role on the performance of the modelled heterojunction cell. The results of the modelled cell have also not changed much on changing the metal contacts at front and back side of the cell. Finally, it has been concluded that if we could reduce the sheet resistance of diamane and can increase its work-function by any technique like chemical doping, then few layers n-diamane can work more efficiently as an emitter layer in Si heterojunction solar cell.

Declaration of Competing Interest

The authors declare that they have no known competing financial interests or personal relationships that could have appeared to influence the work reported in this paper.

CRediT authorship contribution statement

Naima: Conceptualization, Formal analysis, Writing – original draft. **Pawan K. Tyagi:** Conceptualization, Supervision, Writing – review & editing. **Vinod Singh:** Writing – review & editing.

Acknowledgments

The author is thankful to the financial support provided by the Delhi Technological University, new Delhi and authors appreciatively accredited Helmholtz-Zentrum Berlin who provides AFORS-HET simulation software.

References

[1] Z. Zheng, H. Zhan, Y. Nie, X. Xu, D. Qi, Y. Gu, Single layer diamond – a new ultrathin 2D carbon nanostructure for mechanical resonator, Carbon 161 (2020) 809–815.
[2] T. Pakornchote, A. Ektarawong, U. Pinsook, T. Bovornratanaraks, Modifying electronic and elastic properties of 2-dimensional [110]diamond by nitrogen substitution, C J. Carbon Res. 7 (2021).
[3] T. Pakornchote, A. Ektarawong, W. Busayaporn, U. Pinsook, T. Bovornratanaraks, Roles of nitrogen substitution and surface reconstruction in stabilizing non–passivated single-layer diamond, Phys. Rev. B 102 (2020) 075418.
[4] M. Raeisi, B. Mortazavi, E.V. Podryabinkin, F. Shojaei, X. Zhuang, A.V. Shapeev, High thermal conductivity in semiconducting Janus and non-Janus diamanes, Carbon 167 (2020) 51–61.
[5] P.V. Bakharev, M. Huang, M. Saxena, S.W. Lee, S.H. Joo, S.O. Park, J. Dong, D.C. Camacho-Mojica, S. Jin, Y. Kwon, M. Biswal, F. Ding, S.K. Kwak, Z. Lee, R.S. Ruoff, Chemically induced transformation of chemical vapour deposition grown bilayer graphene into fluorinated single-layer diamond, Nat. Nanotechnol. 15 (2020) 59–66.
[6] R.R. Nair, W. Ren, R. Jalil, I. Riaz, V.G. Kravets, L. Britnell, P. Blake, F. Schedin, A.S. Mayorov, S. Yuan, M.I. Katsnelson, H.M. Cheng, W. Strupinski, L.G. Bulusheva, A.V. Okotrub, I.V. Grigorieva, A.N. Grigorenko, K.S. Novoselov, A.K. Geim, Fluorographene: a two-dimensional counterpart of Teflon, Small 6 (2010) 2877–2884.
[7] V.G. Kravets, A.N. Grigorenko, R.R. Nair, P. Blake, S. Anissimova, K.S. Novoselov, A.K. Geim, Spectroscopic ellipsometry of graphene and an exciton-shifted van Hove peak in absorption, Phys. Rev. B 81 (2010) 155413.
[8] F. Piazza, K. Cruz, Raman evidence for the successful synthesis of diamane, Carbon 169 (2020) 129–133.
[9] F. Ke, L. Zhang, Y. Chen, K. Yin, C. Wang, W. Zhu, H. Wang, Y. Lin, Z. Liu, J.S. Tse, G. Wu, R.C. Ewing, W.L. Mao, J. Wu, H.K. Mao, B. Chen, Synthesis and electronic structure characterization of diamane, Condens. Matter Mater. Sci. 10 (2019) 48550.
[10] L. Zhu, W. Li, F. Ding, Giant thermal conductivity in diamane and the influence of horizontal reflection symmetry on phonon scattering, Nanoscale 11 (2019) 4248–4257.
[11] L.A. Chernozatonskii, P.B. Sorokin, A.G. Kvashnin, D.G. Kvashnin, Diamond-like C_2H nanolayer, diamane: simulation of the structure and properties, Condens. Matter 90 (2009) 134–138.
[12] T. Cheng, Z. Liu, Z. Liu, High elastic moduli, controllable bandgap and extraordinary carrier mobility in single-layer diamond, J. Mater. Chem. C 39 (2020) 13819–13826.
[13] J.T. Robinson, J.S. Burgess, C.E. Junkermeier, S.C. Badescu, T.L. Reinecke, F.K. Perkins, M.K. Zalalutdniov, J.W. Baldwin, J.C. Culbertson, P.E. Sheehan, E.S. Snow, Properties of fluorinated graphene films, Nano Lett. 10 (2010) 3001–3005.
[14] K.J. Rietwyk, S.L. Wong, L. Cao, K.M. O'Donnell, L. Ley, A.T.S. Wee, C.I. Pakes, Work function and electron affinity of the fluorine-terminated (100) diamond surface, Appl. Phys. Lett. 102 (2013) 091604.
[15] R. Stangl, C. Leendertz, J. Haschke, Numerical simulation of solar cells and solar cell characterization methods: the open-source on demand program AFORS-HET, Solar Energy, Intech Open, 2010 ch. 14.
[16] K. Patel, P.K. Tyagi, Multilayer graphene as a transparent conducting electrode in silicon heterojunction solar cells, AIP Adv. 5 (2015) 077165.
[17] M.M. Abd El-Raheem, H.M. Ali, N.M. Al-Hosiny, M.S. Abd el aal, Improment of the optical properties of ITO/SiO_2/glass films for photovoltaic applications, J. Non Oxide Glas. 2 (2010) 67–76.
[18] T. Ohshima, T. Matsunaga, H. Kawasaki, Y. Suda, Y. Yagyu, Preparation of ITO thin films by pulsed laser deposition for use as transparent electrodes in electrochromic display devices, Trans. Mater. Res. Soc. Jpn. 35 (2010) 583–587.
[19] S. Zare, H. Izadkhah, C. Vittoria, Deposition of magnetoelectric hexaferrite thin films on substrates of silicon, J. Magn. Magn. Mater. 420 (2016) 245–248.
[20] S.Y. Lien, Characterization and optimization of ITO thin films for application in heterojunction silicon solar cells, Thin Solid Films 518 (2010) S10–S13.
[21] C.K. Borah, P.K. Tyagi, S. Kumar, The prospective application of a graphene/MoS_2 heterostructure in Si-HIT solar cells for higher efficiency, Nanoscale Adv. 2 (2020) 3231–3243.
[22] S.D. Sarma, S. Adam, E.H. Hwang, E. Rossi, Electronic transport in two-dimensional graphene, Rev. Mod. Phys. 83 (2011) 407–470.
[23] Z. Lin, B.R. Carvalho, E. Kahn, R. Lv, R. Rao, H. Terrones, Defect engineering

of two-dimensional transition metal dichalcogenides, 2D Materials 3 (2016) 022002.
[24] S. Bouzidi, M. Barhoumi, M. Said, Optical properties of Janus and non-Janus diamanes monolayers using ab-initio calculations, Optik 235 (2021) 166642.
[25] J. Singh, Semiconductor Devices: Basic Principles, 2nd ed., Wiley India (P) Ltd, New Delhi, 2004.
[26] C.K. Borah, P.K. Tyagi, S. Kumar, K. Patel, Few-layer p-type phosphorene sheet: an efficient transparent conducting electrode in silicon heterojunction solar cell, Comput. Mater. Sci. 151 (2018) 65–72.
[27] Q. Wang, M.R. Page, E. Iwaniczko, Y.Q. Xu, L. Roybal, R. Bauer, B. To, H.C. Yuan, A. Duda, Y.F. Yan, Crystal silicon heterojunction solar cells by hot-wire CVD, Conf. Rec. IEEE Photovolt. Spec. Conf. (2008).
[28] U. Gangopadhyay, S. Roy, S. Garain, S. Jana, S. Das, Comparative simulation study between n-type and p-type Silicon Solar Cells and the variation of efficiency of n-type Solar Cell by the application of passivation layer with different thickness using AFORS HET and PC1D, IOSR J. Eng. 8 (2012) 41–48.
[29] S. Xu, X. Zeng, W. Wang, G. Zhou, Y. Hu, S. Wu, Y. Zeng, Simulation and optimization characteristic of novel MoS_2/c-Si HIT solar cell, J. Min. Mat. Char. Eng. 5 (2017) 323–338.
[30] M. Lundstrom, Heterostructure fudamentals (electronegatividad de electrones), PDF 1995 p. 43.
[31] K.K. Nair, J. Jose, A. Ravindran, Analysis of temperature dependent parameters on solar cell efficiency using MATLAB, Int. J. Eng. Dev. Res. 3 (2016) 536–541.
[32] A.V. Sachenko, V.P. Kostylyov, M.V. Gerasymenko, R.M. Korkishko, M.R. Kulish, M.I. Slipchenko, I.O. Sokolovskyi, V.V. Chernenko, Analysis of the silicon solar cells efficiency. Type of doping and level optimization, Semicond. Phys. Quantum Electron. Optoelectron. 19 (2016) 67–74.
[33] R. Bessler, U. Duerig, E. Koren, The dielectric constant of a bilayer graphene interface, Nanoscale Adv. 1 (2019) 1702–1706.
[34] Y. Zhao, C. Liang, M. Sun, Q. Liu, D.Li F.Zhang, Z. He, Effect of doping on the short-circuit current and open-circuit voltage of polymer solar cells, AIP 116 (2014) 154506.
[35] D. Hamdani, S. Prayogi, Y. Cahyono, G. Yudoyono, D. Darminto, The effects of dopant concentration on the performances of the a-SiO_x:H(p)/a-Si:H(i_1)/a-Si:H(i_2)/μc-Si:H(n) heterojunction solar cell, Int. J. Renew. Energy Dev. 11 (2022) 173–181.
[36] A. Belfar, The role of p+-layer dopant concentration, p+-layer band gap and p+-layer thickness in the performances of a-Si: H n – i – p – p+ solar cells with double layer window nanocrystalline silicon, Optik 126 (2015) 5688–5693.
[37] N. Jensen, R.M. Hausner, R.B. Bergmann, J.H. Verner, U. Rau, Optimization and characterization of amorphous/crystalline silicon heterojunction solar cells, Prog. Photovolt. Res. Appl. 10 (2002) 1–13.
[38] M. Belarbi, M. Beghdad, A. Mekemeche, Simulation and optimization of n-type interdigitated back contact silicon heterojunction (IBC-SiHJ) solar cell structure using Silvaco Tcad Atlas, Sol. Energy 127 (2016) 206–215.
[39] Y. Zhou, G. Long, Low density of conduction and valence band states contribute to the high open-circuit voltage in perovskite solar cells, J. Phys. Chem. C 121 (2017) 1455–1462.
[40] X. Miao, S. Tongay, M.K. Petterson, K. Berke, A.G. Rinzler, B.R. Appleton, A.F. Hebard, High efficiency graphene solar cells by chemical doping, Nano Lett. 12 (2012) 2745–2750.
[41] S.M. Sze, Physics of Semiconductor Devices, 2nd ed., A Willey Interscience Publication, Singapore, 1981.